NOVEL TOOLS FOR IN-BEAM PROTON–GAMMA COINCIDENCE SPECTROSCOPY NEAR $N = Z$*

Y. Hrabar[a], P. Golubev[a], D. Rudolph[a], L.G. Sarmiento[a]
C. Müller-Gatermann[b], W. Reviol[b], D. Seweryniak[b], J. Wu[b,†]
H.M. Albers[c], J.T. Anderson[b], M.A. Bentley[d]
M.P. Carpenter[b], C.J. Chiara[e], P.A. Copp[b,‡], D.M. Cox[a]
C. Fahlander[a], U. Forsberg[a,§], T. Huang[b,¶], H. Jayatissa[b,‡]
T. Lauritsen[b], X. Pereira-Lopez[d,‖], S. Stolze[b]
S. Uthayakumaar[d,††], G.L. Wilson[b,f,‡‡]

[a]Department of Physics, Lund University, 22100 Lund, Sweden
[b]Physics Division, Argonne National Laboratory, Lemont, Illinois 60439, USA
[c]GSI Helmholtzzentrum für Schwerionenforschung, 64291 Darmstadt, Germany
[d]School of Physics, Engineering and Technology, University of York
Heslington, York, YO10 5DD, United Kingdom
[e]U.S. Army Combat Capabilities Development Command Army Research Laboratory, Adelphi, Maryland 20783, USA
[f]Department of Physics & Astronomy, Louisiana State University
Baton Rouge, Louisiana 70803, USA

Received 30 August 2024, accepted 11 February 2025, published online 10 April 2025

A novel combination of two CD-shaped double-sided silicon strip detectors (DSSD) with Gammasphere, Microball, Neutron Shell, and Fragment Mass Analyzer has been exploited at the Argonne Tandem Linac Accelerator System (ATLAS) facility at the Argonne National Laboratory during an experimental campaign aiming to study proton-unbound states in odd-Z,

* Presented at the 57$^{\text{th}}$ Zakopane Conference on Nuclear Physics, *Extremes of the Nuclear Landscape*, Zakopane, Poland, 25 August–1 September, 2024.

† Current address: Brookhaven National Laboratory, Brookhaven, USA.
‡ Current address: Physics Division, Los Alamos National Laboratory, Los Alamos, USA.
§ Current address: Cyclife Sweden AB, Nyköping, Sweden.
¶ Current address: Institute of Modern Physics, Chinese Academy of Sciences, Lanzhou 730000, China.
‖ Current address: Center for Exotic Nuclear Studies, Institute for Basic Science, Daejeon, Republic of Korea.
†† Current address: Facility for Rare Isotope Beams, Michigan State University, East Lansing, USA.
‡‡ Current address: United Kingdom Atomic Energy Authority, Abingdon, United Kingdom.

$N < Z$ nuclei beyond ^{56}Ni. The addition of the highly-pixelated DSSDs to the setup has improved its sensitivity and selectivity for in-beam proton–γ coincidence spectroscopy. Proton tracking capabilities of the DSSD system have been utilized for the first time to follow the beam-spot location on the target, which refines the computation of recoil vectors and thus proton-line energy resolution. Moreover, the high granularity of the DSSD system made it sensitive to unambiguously distinguish evaporated deuterons from evaporated protons. This enables unprecedented deuteron–γ coincidence studies along the $N = Z$ line.

DOI:10.5506/APhysPolBSupp.18.2-A20

1. Introduction

The discrete-energy prompt proton and α emission from excited states, observed and confirmed in several $N \approx Z$ nuclei near $A \approx 60$, is of interest for nuclear theory. Competing electromagnetic and nuclear decay modes of quasi-bound states offer subtle insights into the structure and properties of exotic, unstable nuclei. Experimental knowledge of prompt proton decays has grown since the initial (unexpected) observation in 1998 at the Argonne National Laboratory (ANL) [1]: built upon a $4p$–$4h$ fp-shell excitation across the $N = Z = 28$ shell gap [2, 3], a 9^+ state at the bottom of a well-deformed ($\beta_2 \approx 0.37$) rotational band in $N = Z = 29$ ^{58}Cu was found to decay by emitting a 2.4 MeV, $\ell = 4$, $g_{9/2}$ proton. It connects to the near-spherical neutron $g_{9/2}$ single-particle state in ^{57}Ni [1]. Following this discovery, and a similar case of prompt α emission from deformed states in ^{58}Ni into spherical states of ^{54}Fe [4], a series of dedicated experiments were conducted aiming for high-resolution particle–γ spectroscopy [5]. These employed ΔE–E Si-strip telescope detectors as a central part of their setups to improve the particle's energy resolution. This increased the sensitivity for these rare decay modes at the limit of nuclear stability and allowed to study the decays in greater detail [6–9]. The main factors contributing to experimental uncertainties in the energy resolution of measured proton lines are the intrinsic resolution of the detectors and uncertainties in the computed recoil vector. The former depends on the opening angles of detector elements, the latter on the beam-spot extension and position at the target [5]. This highlights the need for a high-resolution charged-particle detector system including Si detectors to improve the accuracy of determining recoil velocity vectors, and to precisely derive prompt proton energies in the center-of-mass frame.

In a recent experimental campaign at the ATLAS facility at ANL, an upgraded charged-particle setup was placed inside Gammasphere [10]. This upgrade, which is the focus of this paper, comprised two highly-pixelated

CD-shaped double-sided Si strip detectors (DSSD) that were incorporated into the Microball CsI(Tl) detector array [11], and placed inside Gammasphere's target chamber. A schematic drawing is provided in Fig. 1: using the physical space of Microball's ring R4, the DSSD system covers forward angles between $\theta_1 = 12°$ and $\theta_2 = 53°$ with respect to the beam axis. Photos of the upstream DSSD (labeled "DSSD 1" in Fig. 1) and the complete charged-particle system are shown in Fig. 2. The novel setup offers several advantages for proton detection. First, the improved setup has a sufficiently high granularity: 32 rings and 64 sectors give rise to 2048 pixels for each DSSD. This is known to be both decisive and sufficient for improved proton center-of-mass energy resolution from the previous experiments [5, 8, 9]. Second,

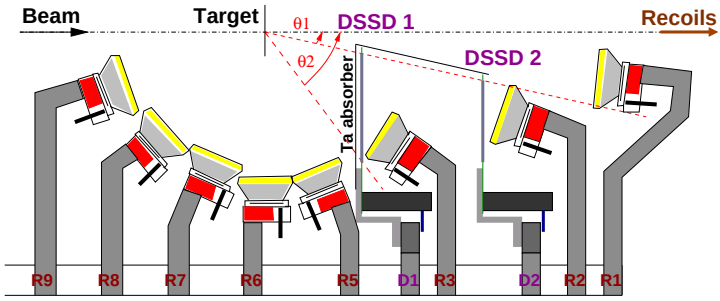

Fig. 1. The combined setup of the Microball CsI(Tl) array and a set of CD-shaped DSSD detectors at the target position. One ring of the Microball array (R4) is removed to fit the DSSD detectors. See the text for additional details.

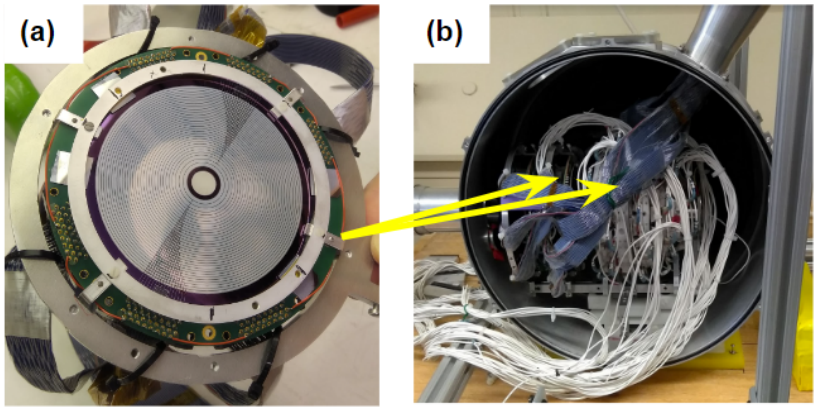

Fig. 2. (Color online) Photo of CD-DSSD 1 detector (a) and the combined setup of the Microball array and the two DSSD detectors inside the target chamber (b). Yellow/light gray arrows indicate the positions of the two DSSDs within Microball. The beam enters the setup from the right.

a high overall charged-particle detection efficiency is preserved by the use of the CsI(Tl) calorimeter. Third, employing the DSSDs adds tracking capabilities by means of multiple, correlated proton hits in the pixelized DSSD system. To allow for the reaction-channel discrimination, the experimental setup also included the Neutron Shell [13], comprising up to 32 liquid scintillator detectors and replacing Gammasphere Ge-detector elements at forward angles, and the Fragment Mass Analyzer (FMA) system for mass over charge ratio, A/Q, determination, and an Ionization Chamber for atomic number, Z, information on recoiling nuclei [14].

This paper is structured as follows: the CD-shaped DSSD system is described in Section 2. Its particle tracking capabilities are presented in Section 3, followed by the description of beam-spot corrections in Section 4. Light charged-particle discrimination achieved due to the upgrade is discussed in Section 5. A brief summary is presented in Section 6.

2. Silicon detectors

The two CD-shaped DSSD with thicknesses of 310 and 520 μm serve as a ΔE–E particle-identification system. The active outer diameter for both detectors is 85 mm. Designed to allow most residual nuclei to pass to the FMA, the wafers have circular openings of 10 mm (DSSD 1) and 28 mm (DSSD 2). This sets the limit for inner active diameters of 14 mm and 32 mm for DSSD 1 and DSSD 2, respectively. Each detector's p-side has 64 sectors. Their n-sides have 32 rings. This creates 2048 pixels per detector [*cf.* Fig. 2 (a) and Fig. 3]. While the DSSD 2 rings are equidistant, the DSSD 1 rings decrease in width from 1.6 mm (innermost) to 1.0 mm (outermost). To protect the DSSDs from scattered beams, a stack of five Ta absorber foils with various diameters and thicknesses was placed in front of DSSD 1. The thickness of the absorbers gradually decreased from 32.5 μm to 12.5 μm [12]. Additionally, a Ta cone was placed through the circular openings of the detectors to provide further shielding.

3. Tracking capabilities

The particle tracking capabilities of the DSSD 1–DSSD 2 system are demonstrated in Fig. 3. By selecting a pixel in DSSD 1 (a), one can identify corresponding pixels in DSSD 2 (b) hit by the same particle ($\Delta t < 50$ ns). The correlations between DSSD 1 and DSSD 2 are consistent with expected ranges of θ (rings) and ϕ (segments) coincident angles based on the kinematics of the reaction induced at the target position (*cf.* Fig. 1). This functionality of the system is then utilized for estimating beam-spot position as described below. Selections in $\Delta\theta$ and $\Delta\phi$ are also used to reduce random background in the ΔE–E-based particle identification.

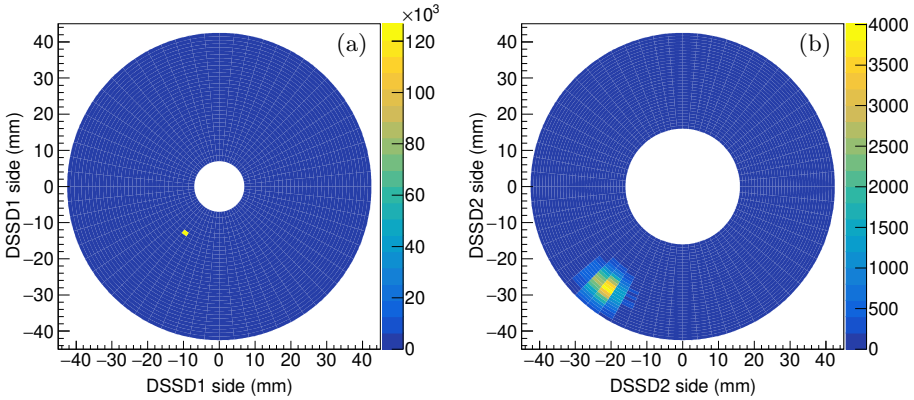

Fig. 3. Particle tracking capabilities of the DSSD system. Shown are selected events which, at the respective detector coordinates, pass through a single pixel in DSSD 1 (a) and share coincidences ($\Delta t < 50$ ns) in DSSD 2 (b).

4. Beam-spot estimation

Accurate control of the beam-spot position as a function of several-day-long experiments is based on particle tracks in the DSSD system on an event-by-event basis. For each ΔE–E-identified proton, two sets of Cartesian coordinates are calculated from the pixel centers where the detectors were hit. Using these coordinates, the proton vector is computed in 3D. The beam-spot X and Y coordinates are then determined, for a defined value of the Z component, at the target position (*cf.* Fig. 1).

Figure 4 shows a resulting 2D hit pattern (bottom left) along with computed beam-spot position coordinates at the target for a representative run (beam tune) of the experiment. If the beam was perfectly centered on the target foil during the run, calculated X and Y coordinates should be close to 0 mm (dashed white lines). However, fitting the X (top left) and Y (bottom right) projections of the histogram indicates $\langle X \rangle = -0.7$ mm and $\langle Y \rangle = -1.2$ mm for the average beam-spot position for the selected data. This is consistent with the beam spot observed on the target foil photo.

Changes in the beam-spot offsets coincided with the beam tuning noted during the experiment. Although the precision of beam-spot estimation is limited by the size of the DSSD pixels, the computed offsets are significant and can be included in the analysis; their scale is compatible with the size of a single DSSD pixel. These offsets would result in a slight change of θ and ϕ angles assigned to particles corresponding to a shift by one pixel. To account for this in further analysis steps, the original θ and ϕ angles for each DSSD pixel computed based on the center of the coordinate system being at (0,0,0) were corrected by θ' and ϕ' computed for the offset beam

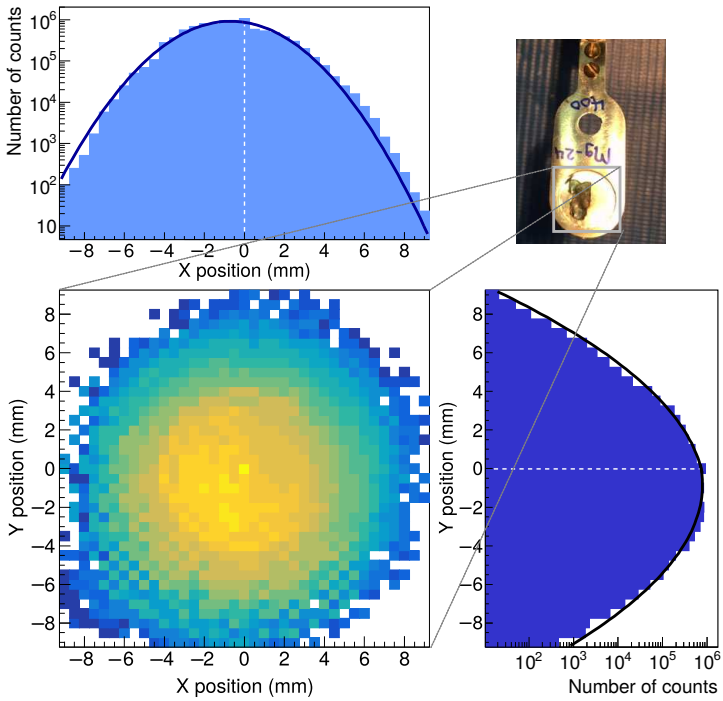

Fig. 4. Calculated beam-spot position coordinates based on proton tracks in the DSSDs for a subset of the data. A 2D hit pattern is shown in the bottom left histogram. The projections for the X and Y coordinates are shown in the top left and bottom right panels of the figure, respectively, with white dashed lines given at 0 mm positions. A photo of the target foil used to take the experiment data is presented in the top right corner.

coordinates. All particles identified in the DSSD system were assigned new beam-spot-corrected angles aiding anticipated in-beam proton–γ coincidence spectroscopy [12, 15].

5. Light charged particle separation

The high granularity of the CD-DSSD system is also beneficial when used as a ΔE–E telescope to distinguish between different types of charged particles. Restricting the range of θ and ϕ spatial correlation in an appropriate way resulted in a very low background in the ΔE–E energy spectra traditionally used for proton–α separation. The spectrum also revealed that the setup is sensitive to deuterons, *i.e.*, the thickness and the geometry of the setup allow for an efficient separation between protons and deuterons, although this was not originally foreseen.

Based on Fig. 1, only the first 14 rings of DSSD 1, counting from the inner aperture, are used for identifying deuterons by means of the present ΔE–E method. The discrimination between protons and deuterons is done, for the DSSD, ring-by-ring, and data selected for a single ring of DSSD 1 is displayed in Fig. 5 (a). This approach helps to reduce the proton and deuteron ΔE–E distributions, caused by the radial change in the Ta absorber foil thickness in front of DSSD 1 as well as the varying effective thicknesses of DSSD 1 itself. Since high-energy protons and deuterons overlap [see Fig. 5 (a)], it is not possible to separate those solely using the DSSDs. This issue can be resolved by further tracking the particles from DSSD 2 into ring 2 of Microball placed directly behind DSSD 2 (see Fig. 1). With DSSD 2 now acting as a ΔE and Microball as an E detector, it is easy to separate those high-energy protons and deuterons as depicted in Fig. 5 (b).

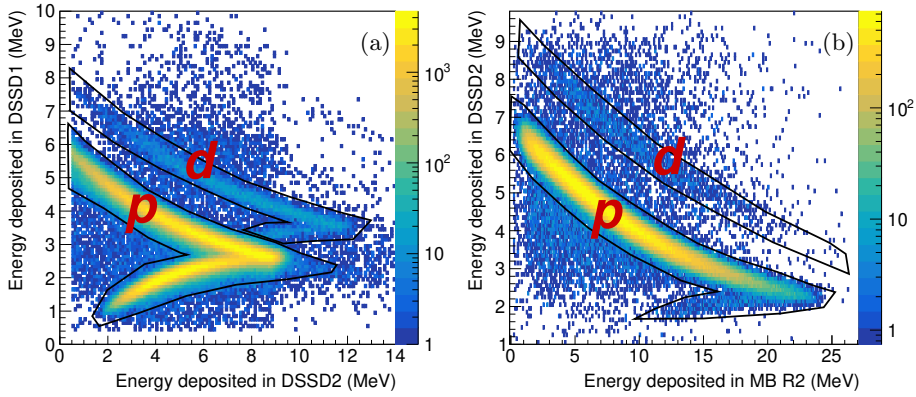

Fig. 5. (a) The sample ΔE–E spectrum plotted for a single DSSD 1 ring (ΔE) and all correlated DSSD 2 rings (E). (b) ΔE–E spectrum obtained by using the combination DSSD 2–Microball ring 2 for high-energy protons and deuterons which are overlapping in energy in panel (a).

6. Summary

Integrating CD-shaped DSSD detectors into the Microball CsI(Tl) array enabled unprecedented proton tracking capabilities, light charged-particle identification, and optimized particle-energy resolution, while maintaining high detection efficiency. The novel setup addressed and advanced on the challenges in estimating the uncertainties of measured prompt proton emission. Specifically, beam-spot estimation was utilized when computing the recoil velocity vector on an event-by-event basis. This resulted in a sharp proton-emission peak of ^{61}Ga discovered during the campaign [12, 15]. Light

charged-particle discrimination allowed for a comprehensive study of deuteron evaporation from a series of compound nuclei along the $N = Z$ line by means of deuteron–γ spectroscopy [12, 16].

We would like to thank the ATLAS accelerator crew for their supreme efforts. This research used resources of ANL's ATLAS facility, which is a DOE Office of Science User Facility. The isotopes used in this research were supplied by the United States Department of Energy Office of Science by the Isotope Program in the Office of Nuclear Physics. This research was funded in part by the Swedish Research Council (Vetenskapsrådet, VR 2016-3969 and VR 2022-3828), the Crafoord Foundation in Lund (grant 20180630), the U.S. Department of Energy, Office of Science, Office of Nuclear Physics (contract No. DE-AC02-06CH11357), and the UKRI Science and Technology Facilities Council under grant numbers ST/P003885/1 and ST/V001035/1.

REFERENCES

[1] D. Rudolph *et al.*, *Phys. Rev. Lett.* **80**, 3018 (1998).
[2] D. Rudolph *et al.*, *Phys. Rev. Lett.* **82**, 3763 (1999).
[3] C. Andreoiu *et al.*, *Eur. Phys. J. A* **14**, 317 (2002).
[4] D. Rudolph *et al.*, *Phys. Rev. Lett.* **86**, 1450 (2001).
[5] D. Rudolph *et al.*, *Eur. Phys. J. A* **14**, 137 (2002).
[6] D. Rudolph *et al.*, *Nucl. Phys. A* **694**, 132 (2001).
[7] D. Rudolph *et al.*, *Phys. Rev. Lett.* **89**, 022501 (2002).
[8] E.K. Johansson *et al.*, *Phys. Rev. C* **77**, 064316 (2008).
[9] E.K. Johansson *et al.*, *Phys. Rev. C* **80**, 014321 (2009).
[10] I.-Y. Lee, *Nucl. Phys. A* **520**, 641c (1990).
[11] D.G. Sarantites *et al.*, *Nucl. Instrum. Methods Phys. Res. A* **381**, 418 (1996).
[12] Y. Hrabar, Ph.D. Thesis, Lund University, Sweden, 2024.
[13] D.G. Sarantites *et al.*, *Nucl. Instrum. Methods Phys. Res. A* **530**, 473 (2004).
[14] C.N. Davids, J.D. Larson, *Nucl. Instrum. Methods Phys. Res. B* **40–41**, 1224 (1989).
[15] Y. Hrabar *et al.*, submitted to *Phys. Rev. Lett.*
[16] Y. Hrabar *et al.*, submitted to *Phys. Rev. C.*